# Anodic oxidation of oxalic acid using WOx based anodes

Bock, C.; Smith, A.; MacDougall, Barry



**Publisher's version / Version de l'éditeur:**

*Electrochimica Acta, 48, 1, 2002*

PERGAMON

Electrochimica Acta 48 (2002) 57–67

ELECTROCHIMICA Acta

www.elsevier.com/locate/electacta

# Anodic oxidation of oxalic acid using $WO_x$ based anodes

C. Bock *, A. Smith, B. MacDougall

*National Research Council Canada, Institute for Chemical Process and Environ. Tech. (ICPET), Montreal Road, Ottawa, ON, Canada K1A 0R6*

Received 10 May 2002; received in revised form 22 July 2002

**Abstract**

The electrochemical $(COOH)_2$ oxidation reaction was studied at high potentials (i.e. in the region where $O_2$ is evolved) in acidic, aqueous solutions using conductive $WO_x$ based anodes. The $WO_x$ films used as anodes also contained Pt 'micro'-centers. Comparative oxidation studies were also carried out using antimony doped $SnO_2$ anodes. More rapid $(COOH)_2$ oxidation rates were observed for the $WO_x$ based anodes than for the antimony doped $SnO_2$ anodes. The $(COOH)_2$ oxidation reaction studied under the conditions used in this work was shown to be activation rather than mass transport controlled. The $(COOH)_2$ oxidation rate constant was found to be independent of the applied potential using the $WO_x$ based anodes. This likely suggests that a chemical reaction is involved in the $(COOH)_2$ oxidation reaction. This chemical reaction is also suggested to be the rate determining step in the $(COOH)_2$ to $CO_2$ oxidation reaction. Furthermore, it is believed that the $(COOH)_2$ oxidation reaction involves adsorptive interactions of this organic with the $Pt/WO_x$ anode surface.


*Keywords:* Anodic oxidation; Oxalic acid; Tungsten oxide anodes; Oxidation mechanism; Kinetics

## 1. Introduction

The use of electrochemical methods for the oxidative removal of organic pollutants from wastewater has attracted much attention [1–4]. It has been shown that toxic organic compounds can be removed from aqueous solutions using metal oxide anodes [1]. This anodic electrolysis process, carried out at high anodic currents where the $O_2$ evolution reaction (oer) also occurs, is referred to as 'anodic oxidation' in this work. The type of anode has been found to influence the reaction pathway. It has been observed that phenol is oxidized to lower aliphatic acids such as oxalic and maleic acid, which are further oxidized to $CO_2$ using antimony doped tin oxide anodes (referred to as SnSb in this work), while phenol is also oxidized to lower aliphatic acids, which are, however, not observed to be oxidized to $CO_2$ using Pt-oxide and $IrO_2$ anodes [2]. This influence of the anode material on the product distribution has been suggested to be due to different concentrations of hydroxy radicals that are being produced as intermediate species in the oer, on the anode surface. In fact, it has been suggested that the observed oxidation of the lower aliphatic acids (oxalic acid, etc.) to $CO_2$ is due to a high hydroxy radical concentration on the SnSb anode surface, while only low hydroxy radical concentrations are suggested to be present at the Pt-oxide and $IrO_2$ anode surfaces; hence, compounds such as oxalic acid are not oxidized to $CO_2$. This proposed reaction mechanism suggests that aliphatic acids such as $(COOH)_2$ may be good test molecules to obtain initial information about the performance of a potential anode material for the oxidation of organics. The reaction mechanism for small molecules is likely less complicated than for large aromatic molecules such as phenol that are well known to have multiple reaction pathway possibilities [5]. Therefore, the use of small test molecules is expected to allow for an easier understanding of the reaction mechanism of this anodic oxidation process.

In previous work [6] the potential use of tungsten oxide ($WO_x$) based anode catalysts, as a novel anode material for the anodic oxidation of organics, has been discussed. It has been shown that these $WO_x$ based anode catalysts that also contain 'micro'-centers of a foreign metal such as Pt or Sn show promising catalytic

* Corresponding author. Tel.: +1-613-990-2252; fax: +1-613-941-2529

*E-mail address:* christina.bock@nrc.ca (C. Bock).

0013-4686/02/$ - see front matter 
PII: S0013-4686(02)00551-0

properties for the anodic oxidation of HCOOH and $(COOH)_2$. Clear evidence was found that the HCOOH oxidation reaction involves adsorptive interactions of this organic with the anode surface. For the case of the $(COOH)_2$ oxidation reaction, adsorptive interactions of $(COOH)_2$ with the $WO_x$ based anode surface may also take place. However, more detailed studies are needed to support this reaction scheme and understand the anodic $(COOH)_2$ oxidation reaction.

In this work, the anodic oxidation of $(COOH)_2$ is studied using $WO_x$ based anodes that contain Pt 'micro'-centers. General morphological and electrochemical characteristics (equilibrium cyclic voltammograms and Tafel plots for the $O_2$ evolution reaction) are discussed and $(COOH)_2$ oxidation studies using SnSb anodes are also carried out. Reaction rate constants are obtained as a function of the applied potential and for different film thicknesses of the $WO_x$ based anodes. Studies are carried out to clarify whether the $(COOH)_2$ oxidation reaction takes place under activation or mass transport controlled conditions and a possible reaction mechanism for the $(COOH)_2$ oxidation reaction is suggested using the results obtained in the present work.

## 2. Experimental

### 2.1. Preparation of $WO_x$ based anodes

Tungsten oxides ($WO_x$) containing Pt 'micro'-centers (and referred to as Pt/$WO_x$ in this work) were formed electrochemically at −0.645 V versus a saturated calomel electrode (SCE) using a method described elsewhere [6,7]. The oxide films were deposited from a 0.1 M tungsten solution (see below) also containing 8 mM $H_2PtCl_6$ (Alfa Aesar, 99.9% metals basis). The $WO_x$ films were deposited onto $IrO_2$ coated Ti substrates. The $IrO_2$ coating was formed by the thermal decomposition (at 500 °C) of a 0.14 M $IrCl_4$ EtOH solution. The $IrCl_4$ solution was painted onto the Ti substrates using a brush. This procedure (painting and decomposition) was repeated twice resulting in ca. 150 nm thick $IrO_2$ layers. Immediately prior to the formation of the $IrO_2$ layer, the Ti substrates were mechanically polished using sandpaper, ultrasonically cleaned in EtOH, etched in boiling (80 °C) 10 M HCl for 10 min, and then well rinsed with $H_2O$. It is known that tungsten oxide films can be deposited onto a variety of conductive substrates [6,7]. In this work, the oxide films were deposited onto the $IrO_2$ coated Ti substrates, as it is well known that the lifetime of oxide anodes can be enhanced in this manner [8].

The 0.1 M tungsten solution was prepared by slowly dissolving 9.1925 g W-powder (1–5 micron, Alfa Aesar, 99.9% metals basis) in 60 ml $H_2O_2$ (30%, Anachemia). The excess $H_2O_2$ was decomposed by immersing a high surface area Pt gauze into the solution. Afterwards, 150 ml EtOH was added and the solution was finally diluted to 500 ml with $H_2O$.

### 2.2. Cells and electrodes

A three compartment cell, in which the reference electrode was generally separated from the working electrode compartment by a Luggin capillary, was employed for the electrochemical studies. For the organic oxidation studies, an H-cell was used allowing the separation of the working and counter electrodes using a Nafion® 117 (DuPont) membrane. The anodic electrolysis experiments were carried out over periods of less than 8 h to avoid crossover of the organics from the working to the counter electrode compartment. Either an SCE or a mercury sulfate electrode (MSE) was used as reference. In all organic oxidation studies, the MSE was used to avoid $Cl^-$ contamination. All potentials reported in this paper are versus the SCE (−0.435 V vs. MSE) unless otherwise stated. A large surface area Pt gauze served as the counter electrode. In some cases, antimony doped $SnO_2$ (SnSb) (prepared as described previously [1]) and polycrystalline Pt foils (0.1 mm thick, 99.99% metals basis, Alfa Aesar) were also employed as working electrodes. The geometrical area of all working electrodes employed was 0.98 $cm^2$ and electrode areas are referred to as geometrical unless otherwise stated.

### 2.3. Techniques and instrumentation

Electrochemical experiments were performed using either an EG&G 273 potentiostat or a Solarotron SI 1287 electrochemical interface (Solarotron Group, Ltd.) both driven by Corrware software program (Scribner, Assoc.). Ohmic drop compensation was performed when necessary, i.e. for experiments involving high currents using either a 'feedback' or 'sampled' mode. The concentration of the organic species was determined using a HP series 1100 high performance liquid chromatograph (HPLC). An Ion-Interaction column (Mandel), thermostated at 46 °C, was used. The UV detector was set at 195 nm. Sulphuric acid (0.01 M) was used as mobile phase at a flow rate of 0.3 ml $min^{-1}$. A Shimadzu UV-1201 S UV/VIS Spectrophotometer was used to identify possible organic reaction products. A Mitutoyo micrometer was used for the measurement of the thickness of the dry oxide films. A JEOL JSM-5300 Scanning Microscope was also employed to obtain morphological information of the $WO_x$ based films.

### 2.4. Solutions

The majority of the oxidation studies were carried out using $10^{-3}$ M $(COOH)_2$ in 0.5 M $H_2SO_4$ solutions. All $(COOH)_2$ oxidation studies were carried out under

constant potentiostatic conditions. High resistivity (18 MΩ) $H_2O$ and A.C.S. grade chemicals were used. High purity argon gas was used to deoxygenate the electrolyte solution and all electrochemical experiments were performed at room temperature. The electrolysis solutions were well stirred using a magnetic stirring bar and a Corning stirring plate.

## 3. Results and discussion

### 3.1. Electrochemical characteristics and morphology of the Pt/$WO_x$ anodes

Fig. 1 shows typical current density (J)–potential (V) characteristics for two Pt/$WO_x$ electrodes deposited for 40 and 120 min, respectively. Both anodes were conditioned for 7 days in 2 M $H_2SO_4$ at $10^{-2}$ A $cm^{-2}$, as discussed below. At lower potentials, between −0.3 and 0.3 V, the electrochemical $WO_x$ film conversion reaction takes place as follows [7]:

$$WO_3 + xH^+ + xe^- = H_xWO_3 \quad (1)$$

This reaction is superimposed on the $H_2O$ adsorption/desorption reaction that takes place on the Pt sites. In fact, the typical characteristics for polycrystalline Pt are recognizable in the two cyclic voltammograms (CVs) of the Pt/$WO_x$ anodes. At more positive potentials the electrochemical formation of PtO is recognizable in the anodic scan. The PtO is reduced to metallic Pt in the cathodic scan. Cycling up to 1.09 V in 0.5 M $H_2SO_4$ results in the formation of one monolayer of PtO [6,9]. Therefore, the PtO to Pt reduction peak can be used to obtain an estimate of the electro-active Pt area within the $WO_x$ film using a conversion of 420 μC per $cm^2$ Pt [9]. It is seen (Fig. 1) that Pt/$WO_x$ films containing very high surface electro-active Pt areas, in these two cases of ca. 105 and 310 $cm^2$, are formed employing deposition times of 40 and 120 min, respectively. The dry oxide

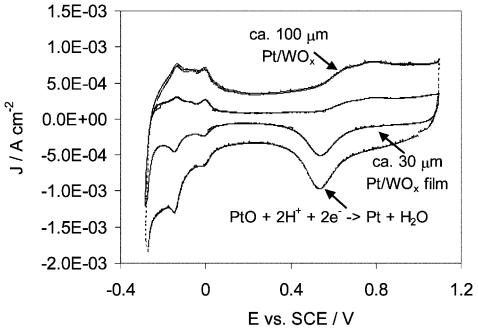


Fig. 1. Typical cyclic voltammograms of conditioned Pt/$WO_x$ films in quiescent 0.5 M $H_2SO_4$ recorded at 2 mV $s^{-1}$. The Pt/$WO_x$ films were deposited onto Ti/$IrO_2$ substrates at −0.645 V vs. SCE for 40 and 120 min resulting in dry film thicknesses of ca. 30 and 100 μm, as indicated in Fig. 1. After deposition, the films were conditioned in 2 M $H_2SO_4$ at $10^{-2}$ A $cm^{-2}$ for 7 days.

thicknesses are ca. 30 and 100 μm for the films deposited for 40 and 120 min, respectively. The $WO_x$ films are good conductors and are stable in $H_2SO_4$ solutions even at 'high' current densities [6]. Initial changes in the oxide film structure take place when these oxides are used as $O_2$ evolving anodes, as indicated by the changes in the CV characteristics of a particular oxide film recorded before and after its use as an $O_2$ evolving anode [6]. It has been found that steady-state cyclic voltammogram (CV) characteristics are obtained after an initial period of 4 days of electrolysis at $10^{-2}$ A $cm^{-2}$ in 2 M $H_2SO_4$ [6]. Therefore, all $WO_x$ electrodes studied in this work were conditioned in 2 M $H_2SO_4$ at $10^{-2}$ A $cm^{-2}$ for 7 days before they were used as anodes for the $(COOH)_2$ oxidation studies. Furthermore, all oxidation studies reported in this work were carried out at high potentials, thus the oer also took place to different extents.

Fig. 2 shows two scanning electron micrographs (SEMs) for the (310 $cm^2$ real Pt area) Pt/$WO_x$ film, i.e. for the same film as used in the CV studies above (Fig. 1). The SEMs show the top views of the black Pt/$WO_x$ anode that has been used as oer anode in prior experiments at two different magnifications of 2k and 5k. At a magnification of 2k (Fig. 2a), a cracked oxide structure is recognizable, thus suggesting easy access of the electrolyte solution into the oxide structure. At higher magnifications of 5k (Fig. 2b), fine structured features are visible and a highly porous oxide, sandstone like film structure is revealed. These results are consistent with the high surface area nature of these Pt/$WO_x$ anodes seen in the CV studies (Fig. 1).

### 3.2. Tafel slopes for the $O_2$ evolution reaction in the absence of organics

Fig. 3 shows typical Tafel plots for the oer on polycrystalline Pt and a (78 $cm^2$ real Pt area) Pt/$WO_x$ anode recorded in 0.5 M $H_2SO_4$. The Tafel plots for the Pt electrode were obtained following a method described previously [10]. For these measurements the applied current densities were decreased successively from $5 \times 10^{-2}$ to $5 \times 10^{-6}$ A $cm^{-2}$, as discussed elsewhere [10]. This approach was adopted in order to ensure that the nature of the electrode surface was reasonably constant during the polarization measurements. By going from the higher to lower anodic currents, or potentials, the more stable Pt surface oxides formed at the higher potentials will tend to be 'locked-in' since a considerable hystersis exists between oxide formation and reduction. The 'constant' nature of the Pt surface, and its oxides, will help to ensure reproducible and meaningful Tafel slopes [10,11]. In this work, steady-state potential measurements were obtained after 20 min. An experimental Tafel slope value of 120 (±3) mV $dec^{-1}$ was found for the Pt electrode. This value is in good agreement with literature data and indicates that an

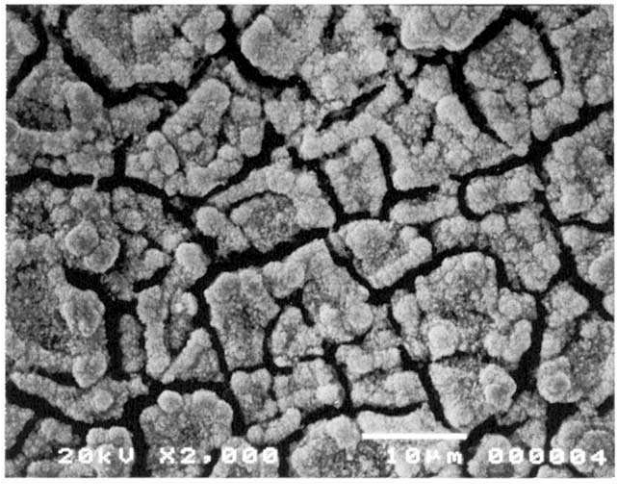


(a)

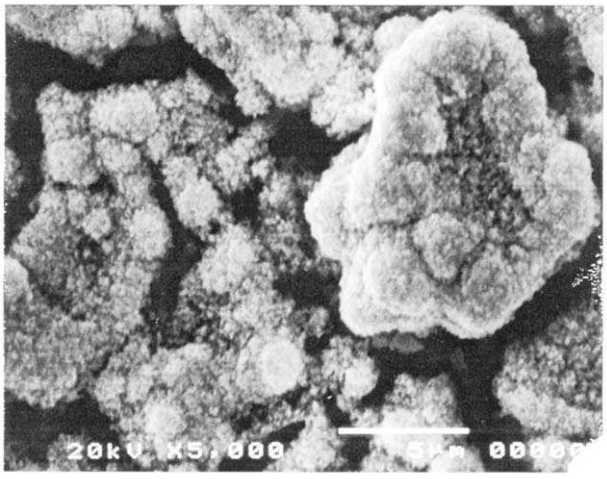


(b)

Fig. 2. SEMs for a (310 $cm^2$ real Pt area) Pt/$WO_x$ anode. Fig. 2a, shows the top view of the oxide electrode at 2k time magnification, while Fig. 2b shows the same for a 5k time magnification. The Pt/$WO_x$ anode was used as an oer anode in $H_2SO_4$ solutions at high current densities.

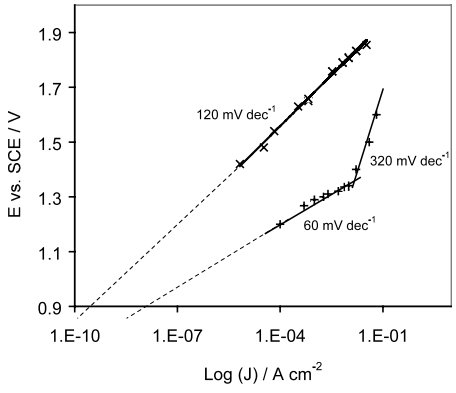


Fig. 3. Tafel plots for the $O_2$ evolution reaction in quiescent 0.5 M $H_2SO_4$ for polycrystalline Pt ( × ) and (78 $cm^2$ real Pt area) Pt/$WO_x$ (+) anodes.

initial one electron electrochemical reaction is rate determining [10]. For the Pt/$WO_x$ anodes, two regions of different Tafel slopes appear to exist. The value for the Tafel slope at lower potentials is seen to be 60 ($\pm$3) mV $dec^{-1}$, while a value of 320 mV $dec^{-1}$ is found at higher potentials. The very large Tafel slope value of 320 mV $dec^{-1}$ could indicate that a resistive film on e.g. the underlying titanium substrate is formed under these harsh conditions of high currents and rapidly evolving $O_2$. The change in Tafel slope for the Pt/$WO_x$ anode is seen to take place at ca. 1.4 V. This potential is possibly the upper limit at which the $WO_x$ films made in this work should be used as anodes. Therefore, the $WO_x$ based anodes were not used at very positive potentials. Since the evaluation of the exact mechanism of the oer was not the purpose of this work, the Tafel slope data are not further evaluated. However, it should be mentioned that the different oer Tafel slopes observed for the Pt and Pt/$WO_x$ anodes may have implications for the organic oxidation mechanisms at these two anodes. It should be noted that thermally prepared $IrO_2$ anodes typically show a Tafel slope of 60 mV $dec^{-1}$ in acidic solutions and one may assume that the lower Tafel slope observed for the anodes studied in this work is related to the thin $IrO_2$ underlayer [12]. However, in this work it was observed that at a particular potential the currents for Pt/$WO_x$ anodes increase in a proportional manner with increasing Pt/$WO_x$ film thickness, i.e. with increasing Pt area. Therefore, it is probable that the experimentally observed Tafel slope of 60 mV $dec^{-1}$ reflects the $O_2$ evolution reaction for the thick Pt/$WO_x$ layer.

The exchange current density ($J_o$) values for the oer were also obtained for the Pt and the Pt/$WO_x$ anodes by extrapolating the experimental potential–log current density data to the theoretical zero overpotential value of 1.23 V versus RHE (0.9 V vs. SCE in 0.5 M $H_2SO_4$) [10], as shown in Fig. 3. For the Pt and the Pt/$WO_x$ anodes, $J_o$ values of $4\pm2\times10^{-10}$ and $4\pm2\times10^{-8}$ A $cm^{-2}$, respectively, were found. The former is in good agreement with the literature [10]. The $J_o$ value for the Pt/$WO_x$ anode is 100 times larger than for the Pt electrode, which is most likely due to the high surface area of the tungsten oxide based anode. The results likely suggest that the oer takes place on the Pt sites within the $WO_x$ film, since the real Pt area of the $WO_x$ anode used here is ca. 80 times larger than the real area of the polycrystalline Pt electrode, i.e. close to the 100 times observed difference in the $J_o$ values.

### 3.3. Anodic $(COOH)_2$ oxidation at high potentials

#### 3.3.1. Current density–time profiles as a function of the $(COOH)_2$ concentration

Fig. 4 shows typical current density–time profiles as a function of increasing $(COOH)_2$ concentration using Pt/

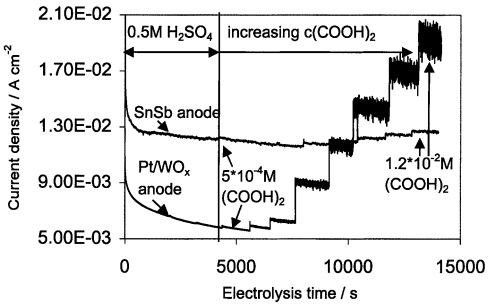


Fig. 4. Typical current density–time profiles as a function of the $(COOH)_2$ concentration for a $Pt/WO_x$ anode of 58 $cm^2$ real Pt area and a SnSb anode. The experiments were carried out at 1.385 and 1.885 V vs. SCE using $Pt/WO_x$ and the SnSb anodes, respectively in rigorously stirred solutions. An MSE was used in the actual experiments. The $(COOH)_2$ concentration was increased from $5 \times 10^{-4}$ to $1.2 \times 10^{-2}$ M in $1.6 \times 10^{-3}$ M increments.

$WO_x$ (58 $cm^2$ real Pt area) and SnSb anodes, recorded at 1.385 and 1.885 V, respectively. For the $Pt/WO_x$ anode, the current was found to increase with increasing $(COOH)_2$ concentration in a linear manner, indicating a first order dependence of the $(COOH)_2$ oxidation rate on concentration. The monitored current density is ca. three times larger for the $1.2 \times 10^{-2}$ M $(COOH)_2$ solution than for the 0.5 M $H_2SO_4$ background solution, indicating electrocatalytic acitivity of these $Pt/WO_x$ anodes for the $(COOH)_2$ oxidation reaction. The current for the SnSb anode is seen to also increase with increasing $(COOH)_2$ concentration, however, the increase in the current density is less pronounced than observed for the $Pt/WO_x$ anode. Electrolysis experiments carried out using the SnSb anode at lower potentials, and hence involving lower currents, also resulted in only small increases in the current density with increasing $(COOH)_2$ concentration. These results suggest that the $(COOH)_2$ oxidation rate is more rapid for the $Pt/WO_x$ than the SnSb anode. Furthermore, in parallel work, $CO_2$ measurements showed that $(COOH)_2$ is quantitatively oxidized to $CO_2$ using these $Pt/WO_x$ anodes [6]. The $Pt/WO_x$ anodes are thus good electro-catalysts for the oxidation of $(COOH)_2$ to $CO_2$.

### 3.3.2. $(COOH)_2$ oxidation rate constants

It has been shown from preliminary $(COOH)_2$ oxidation studies, carried out in previous work under similar electrolysis conditions [6], that the $(COOH)_2$ oxidation reaction using $Pt/WO_x$ anodes follows first order reaction kinetics. The first order rate constant ($k_1$) was estimated from the concentration/time profiles, i.e. ($\ln(c_o/c_{(t)})$ versus electrolysis time plots, $c_o$ being the initial $(COOH)_2$ concentration and $c_{(t)}$ the $(COOH)_2$ concentration determined at a particular electrolysis time, as a function of the applied potential using high surface area $Pt/WO_x$ anodes. These experiments were carried out at constant potentials and by rigorously stirring the electrolysis solution. The experimentally determined $k_1$ values were observed to not be influenced by the solution stirring rate, suggesting that the $(COOH)_2$ oxidation reaction is activation controlled. However, the simultaneously occurring oer could result in (turbulent) stirring of the electrolyte solution within the oxide film and at the anode surface. If local solution stirring due to the oer is more effective than the mechanical stirring, the observed lack of influence of the latter on the $(COOH)_2$ oxidation rate does not necessarily mean activation control. Indeed, it is possible that the $(COOH)_2$ oxidation reaction within the high surface area oxide structure of these $Pt/WO_x$ anodes is mass transport controlled, even with the stirring caused by parallel gas evolution. Under such conditions, the reaction rate constant would be independent of the applied potential, as is indeed shown below. But such a result could also be due to a 'complex' $(COOH)_2$ oxidation reaction mechanism under activation control. In order to establish the 'correct' reason for these results, the dependence of $k_1$ on various systems parameters is carefully studied in the following sections.

*3.3.2.1. J–t profiles: influence of solution stirring rate.* Fig. 5 shows a plot for the average current density ($J_{av}$) versus the solution stirring rate obtained for the electrolysis of 20 ml of a $10^{-3}$ M $(COOH)_2$ in 0.5 M $H_2SO_4$ solution at 1.235 V using a (58 $cm^2$ real Pt area) $Pt/WO_x$ anode. This potential was selected in order to have a reasonably high current efficiency for the $(COOH)_2$ oxidation reaction. The $J_{av}$ data shown in Fig. 5 are the average of the $J$ data collected at a particular stirring rate at 10 s intervals for 5 min. The solution stirring rates were randomly altered and multiple $J_{av}$ data were collected for a number of different

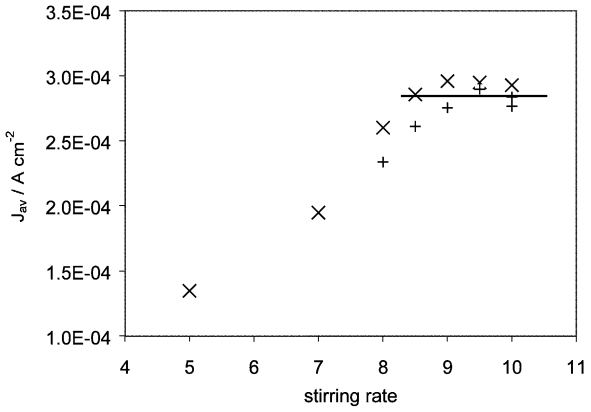


Fig. 5. The influence of the solution stirring rate on the monitored average current density ($J_{av}$) for a (58 $cm^2$ real Pt area) $Pt/WO_x$ anode. A $10^{-3}$ M $(COOH)_2$ in 0.5 M $H_2SO_4$ solution was used. The solution was stirred using a magnetic stirring plat, as described in Section 2. The individual $J_{av}$ values were obtained by averaging the monitored $J$ data over a period of 5 min. The solid straight line indicates the independence of the $J_{av}$ data on the stirring rate.

stirring rates. It is seen that the $J_{av}$ value decreases with decreasing solution stirring rate for rates smaller than 8.5 indicating that the $(COOH)_2$ oxidation reaction is mass transport controlled under these conditions. At higher solution stirring rates than 8.5, the $J_{av}$ value is independent of the stirring rate. This behavior is consistent with an activation controlled mechanism for the $(COOH)_2$ oxidation reaction, provided the stirring rate is sufficiently high. The current density was seen to increase from $5.1 \times 10^{-5}$ A $cm^{-2}$ for the organic free 0.5 M $H_2SO_4$ solution to ca. $3 \times 10^{-4}$ A $cm^{-2}$ for the 'presumably' activation controlled reaction of the $10^{-3}$ M $(COOH)_2$ solution. This is an increase in current density of ca. five times upon the addition of $(COOH)_2$. This indicates that the majority of the monitored current is due to the oxidation of $(COOH)_2$ to $CO_2$ (as opposed to the oer), as further discussed below.

*3.3.2.2. $k_1$ and $I_{eff}$ dependence on the applied potential.* In this section, the influence of the applied potential on the $(COOH)_2$ oxidation reaction rate constant is investigated for a $Pt/WO_x$ anodes (58 $cm^2$ real Pt area). For the electrolysis studies, 20 ml's of $10^{-3}$ M $(COOH)_2$ in 0.5 M $H_2SO_4$ solution was used and the solution was rigorously stirred (i.e. using a stirring rate larger than 9.5), as discussed above. The $k_1$ values were estimated from the slope of $\ln(c_o/c_{(t)})$ versus electrolysis time plots, as discussed in previous work [6]. Half-life times ($\tau_{1/2}$) were also estimated. The $\tau_{1/2}$ values were estimated from the $(COOH)_2$ concentration versus electrolysis time plots when the $(COOH)_2$ concentration reached half of its original value [13]. Table 1 shows $k_1$ and $\tau_{1/2}$ values for the $Pt/WO_x$ anode as a function of the applied potential. It is seen that both the $k_1$ and $\tau_{1/2}$ values are independent of the applied potential. However, it should be noted that essentially the same $k_1$ and $\tau_{1/2}$ values were also found when different solution stirring rates (0.85–1) were employed at a particular potentials. In conjunction with the result from Fig. 5, it appears that the reaction is activation rather than a mass transport controlled reaction. Therefore, the potential independence of $k_1$ and $\tau_{1/2}$ is most probably not simply due to mass transport control of the reaction. There is good reproducibility of the $k_1$ and $\tau_{1/2}$ data, and it appears that the $Pt/WO_x$ anode is stable and not altered by the $(COOH)_2$ oxidation reaction, at least on the experimental time scale tested here.

Table 1
$(COOH)_2$ oxidation data as a function of potential using a (58 $cm^2$ real Pt area) $Pt/WO_x$ anode

| $E$ vs. SCE [a] (V) | $k_1$ [b] ($s^{-1}$) | $\tau_{1/2}$ [b] (h) |
|---|---|---|
| 1.235 | $5.3\ (\pm 0.6) \times 10^{-5}$ | 4 |
| 1.285 | $5.8\ (\pm 0.6) \times 10^{-5}$ | 4 |
| 1.335 | $5.3\ (\pm 0.6) \times 10^{-5}$ | 4 |
| 1.385 | $5.5\ (\pm 0.6) \times 10^{-5}$ | 4 |

The $k_1$ and $\tau_{1/2}$ values are extracted from experimental concentration–time profiles for rigorously stirred solutions, as described in the text.

[a] The potentials are referred to vs. an SCE, even though, an MSE was used in the experiments.

[b] The $k_1$ and $\tau_{1/2}$ values are extracted from the anodic electrolysis data obtained using initially 20 ml's of $10^{-3}$ M $(COOH)_2$ in 0.5 M $H_2SO_4$ solutions, as described in the text.

Fig. 6 shows the dependence of the current efficiency ($I_{eff}$) on the electrolysis time for four different potentials. The $I_{eff}$ values were calculated by dividing the theoretical charge needed to oxidize a measured amount of $(COOH)_2$ to $CO_2$ ($Q_{th(organic \rightarrow CO_2)}$) with the experimental charge passed within a specific time interval in the electrolysis experiment ($Q_{exp}$), i.e.:

$$I_{eff} = 100 \times \frac{Q_{th(organic \rightarrow CO_2)}}{Q_{exp}} \quad (2)$$

The $Q_{th(organic \rightarrow CO_2)}$ values were calculated using experimentally observed $(COOH)_2$ concentration changes monitored for particular electrolysis time intervals of 1 h, i.e. for the same time interval as used for the $I_{eff}$ data calculations shown in Fig. 6. Fig. 6 shows that, for a particular electrolysis time, the $I_{eff}$ values decrease as the potential is made more positive, indicating that the fraction of the total current corresponding to the oer increases with increasing potential. At lower potentials, namely at 1.235 and 1.285 V, the $I_{eff}$ values are seen to be very high; in some cases current efficiencies of close to 100% are observed during the first one to 3 h of electrolysis. This indicates that the observed current is mostly due to oxidation of $(COOH)_2$ and that the fraction of the current towards the oer is small.

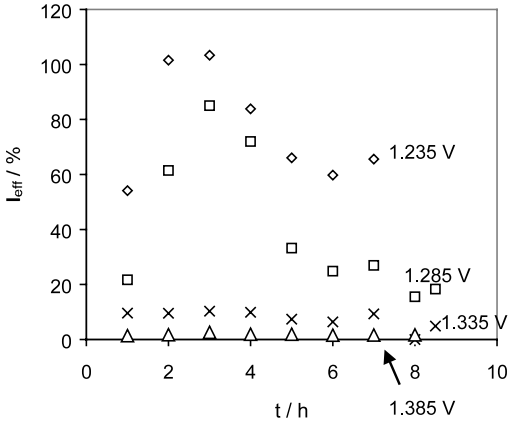


Fig. 6. Current efficiencies ($I_{eff}$) values for the $(COOH)_2$ to $CO_2$ oxidation as a function of the electrolysis time. A (58 $cm^2$ real Pt area) $Pt/WO_x$ anode was used and the $I_{eff}$ values were estimated using experimental data collected during 1 h time intervals at: (◇), 1.235; (□), 1.285; (×), 1.335; and (△) 1.385 V vs. SCE using Eq. (2). An MSE was employed in the actual experiments. Twenty millilitres of initially $10^{-3}$ M $(COOH)_2$ in 0.5 M $H_2SO_4$ solutions were used for the anodic electrolysis studies. The solutions were rigorously stirred, as described in the text.

Furthermore, the experimentally observed $(COOH)_2$ concentration changes suggest that ca. $2 \times 10^{-5}$ mol's $CO_2$ (which is equivalent to ca. $8 \times 10^{-3}$ $cm^3$ $CO_2$, assuming a gas volume of $24 \times 10^{-3}$ mol $cm^{-3}$ [14]) are evolved during the first hour of electrolysis. These results suggest that neither the evolution of $CO_2$ nor $O_2$ are likely to contribute to the stirring of the electrolyte solution. It appears reasonable to assume that for the conditions employed here, the solution stirring takes place solely by mechanical means. The $I_{eff}$ values are generally seen to decrease with increasing electrolysis time, and hence decreasing $(COOH)_2$ concentration, as one would expect since the rate of the oer is not decreasing. However, the $I_{eff}$ values observed during the initial electrolysis times are found to be consistently smaller than the subsequent $I_{eff}$ value (Fig. 6). The origin of this behavior is not clear. It may arise from a particular $(COOH)_2$ oxidation mechanism, and needs to be further investigated.

*3.3.2.3. Diffusion layer thickness estimation and limiting current density calculation.* In this section, the experimentally observed current densities for the anodic $(COOH)_2$ oxidation are compared to the 'theoretical' limiting current densities ($J_{lim}$) estimated for the oxidation reaction taking place under true mass transport controlled conditions. The $J_{lim}$ value for a mass transport controlled reaction is defined as follows [13]:

$$J_{lim} = \frac{nFcD}{\delta} \quad (3)$$

In Eq. (3), $n$ is the number of electrons, $F$ Faraday's constant, $c$ the concentration of the reactant, $D$ the diffusion coefficient of the reactant and $\delta$ the diffusion layer thickness. The calculation of the $J_{lim}$ value requires knowledge of the diffusion coefficient and the diffusion layer thickness. These two values were estimated in the present work from experimental $(COOH)_2$ oxidation studies carried out at low potentials, i.e. at potentials lower than those needed for the oer using a polycrystalline Pt electrode. The $D$ value for the oxalic acid was first extracted using the experimentally observed dependence of the current density peak maxima ($J_{p,a}$) on the sweep rates. The CV experiments were carried out for a quiescent $10^{-3}$ M $(COOH)_2$ in 0.5 M $H_2SO_4$ solution, the potential being cycled between $-0.245$ and 1.07 V. A D value of $5 (\pm 1) \times 10^{-6}$ $cm^2$ $s^{-1}$ was extracted from the slope of the $J_{p,a}$ versus the square root of the sweep rate ($s^{1/2}$) plot using the well known Randles–Sevcik equation [15], as shown in Fig. 7. The $\delta$ value for the stirred solution (using a mechanical stirring rate of 9.5) was then estimated in a different set of CV experiments for a range of $(COOH)_2$ concentrations, namely $10^{-3}$–$1.6 \times 10^{-2}$ M $(COOH)_2$ in 0.5 M $H_2SO_4$. The same Pt electrode was employed and the potential was cycled at

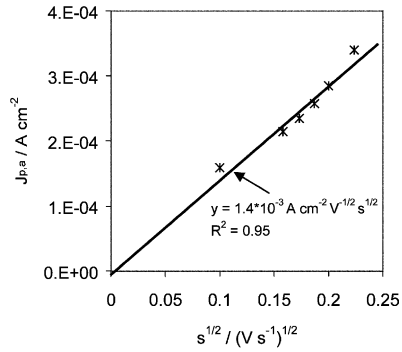


Fig. 7. Dependence of the $(COOH)_2$ oxidation peak maxima ($J_{p,a}$) on the square root of the sweep rate. The $J_{p,a}$ values are extracted from CV experiments recorded between $-0.245$ and 1.07 V vs. SCE in a quiescent $10^{-3}$ M $(COOH)_2$ in 0.5 M $H_2SO_4$ solution. An MSE was used in the actual experiments. A Pt electrode was used for these CV experiments.

10 mV $s^{-1}$ between $-0.245$ and 1.07 V. In all experiments, a limiting current was observed for the $(COOH)_2$ oxidation reaction at potentials more positive than 0.98 V. The $J_{lim}$ value was found to be proportional to the $(COOH)_2$ concentration, as shown in Fig. 8. According to Eq. (3), the slope of this plot is proportional to $nFD/\delta$, i.e. it yields a measurement of the $\delta$ value. For the particular solution stirring conditions employed in this work, the slope of 640 A cm $mol^{-1}$ estimated from Fig. 8 and a $D$ value of $5 (\pm 1) \times 10^{-6}$ $cm^2$ $s^{-1}$ suggests a $\delta$ value of 15 μm. While this value is somewhat lower than reported for a mechanically stirred system [13], the exact value will depend on such important factors as cell geometry. Consequently, the 15 μm value is used below.

The $D$ and $\delta$ values of $5 \times 10^{-6}$ $cm^2$ $s^{-1}$ and 15 μm, respectively, were used to calculate the limiting current density ($J_{lim}$) using Eq. (3) for the anodic $(COOH)_2$

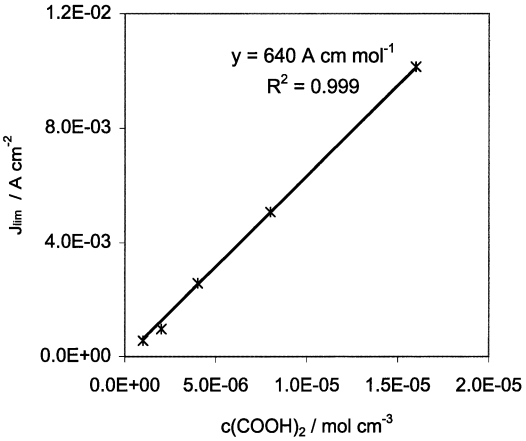


Fig. 8. Dependence of $J_{lim}$ on the $(COOH)_2$ concentration. The $J_{lim}$ values are extracted from CVs recorded for a rigorously stirred (rate of 9.5) $(COOH)_2$ solution in 0.5 M $H_2SO_4$. The potential was cycled at 10 mV $s^{-1}$ between $-0.245$ and 1.07 V vs. SCE. An MSE was used in the actual experiment. A Pt electrode was used for these CV experiments.

electrolysis experiments carried out in this work. These numbers were compared to the average current densities ($J_{exp}$) obtained from the experimentally observed $(COOH)_2$ concentration changes during a particular electrolysis period using Faraday's law and assuming a 2 $e^-$ oxidation reaction. Typical data are shown in Table 2 for the electrolysis of 20 ml's of an originally $10^{-3}$ M $(COOH)_2$ in 0.5 M $H_2SO_4$ solution using a (58 $cm^2$ real Pt area) $Pt/WO_x$ anode. It is seen that for the entire period of this particular 6 h electrolysis experiment, the $J_{exp}$ is smaller than the $J_{lim}$ value. In fact, the $J_{exp}$ value is seen to be consistently smaller (by ca. three times) than the $J_{lim}$ value. It is very important to note that the $J_{exp}$ values are based on the geometrical area of the $Pt/WO_x$ anode, not the real surface area (since we do not know for certain the number as well as the nature of the catalyst site that are utilized [6]). If a roughness factor of 58 was used, the $J_{exp}$ values would be that much lower, and the three times difference factor would be more like 175 times (the $J_{lim}$ values were based on a 1 $cm^2$ Pt electrode). In any case, the real surface area of the $Pt/WO_x$ anode is likely more than the 1 $cm^2$, and hence, the difference between the true current density and the $J_{lim}$ value is expected to be more than the three times cited in Table 2. Based on these arguments, the results are believed to be consistent with a mainly activation controlled mechanism and add support to the activation rather than mass transport controlled mechanism suggested for the $(COOH)_2$ oxidation reaction studied here.

Table 2
$J_{exp}$ and $J_{lim}$ values as a function of the $(COOH)_2$ concentration ($c_{(t)}$) [a]

| Electrolysis period (h) | $c_{(t)}$ [b] (M) | $J_{exp}$ [c] (A $cm^{-2}$) | $J_{lim}$ [d] (A $cm^{-2}$) | $J_{lim(calc)}/J_{exp}$ |
|---|---|---|---|---|
| 0–1 | $8.6 \times 10^{-4}$ | $1.6 \times 10^{-4}$ | $5.6 \times 10^{-4}$ | 3.5 |
| 1–2 | $7.4 \times 10^{-4}$ | $1.4 \times 10^{-4}$ | $4.7 \times 10^{-4}$ | 3.5 |
| 2–3 | $6 \times 10^{-4}$ | $1.4 \times 10^{-4}$ | $3.9 \times 10^{-4}$ | 3 |
| 3–4 | $5 \times 10^{-4}$ | $1.3 \times 10^{-4}$ | $3.1 \times 10^{-4}$ | 2.5 |
| 4–5 | $4.8 \times 10^{-5}$ | $9.5 \times 10^{-5}$ | $2.6 \times 10^{-4}$ | 3 |
| 5–6 | $4 \times 10^{-5}$ | $8.2 \times 10^{-5}$ | $2.2 \times 10^{-4}$ | 2.5 |

[a] Electrolysis experiments were carried out at a constant potential of 1.335 V vs. SCE, although, an MSE was employed in the actual experiment. The solutions were rigorously stirred, as described in the text. A (58 $cm^2$ real Pt area) $Pt/WO_x$ anode was used. Twenty millilitres of an initially $10^{-3}$ M $(COOH)_2$ and 0.5 M $H_2SO_4$ solution was used for the electrolysis experiment.

[b] The $(COOH)_2$ concentrations ($c_{(t)}$'s) were determined as a function of the electrolysis time by HPLC.

[c] The $J_{exp}$ values are the average current densities for the $(COOH)_2$ to $CO_2$ oxidation. The latter were obtained by averaging the current densities estimated for a particular electrolysis period, as indicated (column 1), from experimentally observed $(COOH)_2$ concentration changes using Faradays law and assuming a 2 $e^-$ oxidation reaction. The geometrical electrode area (0.98 $cm^2$) was used as opposed to the real area.

[d] The $J_{lim}$ values are limiting current densities calculated for a 2 $e^-$ oxidation reaction that is mass transport controlled. The $J_{lim}$ values are calculated using Eq. (3), the $c(COOH)_2$ concentrations given in Table 2 (column 2), a $D$ value of $5 \times 10^{-6}$ $cm^2$ $s^{-1}$ and a $\delta$ value of 15 μm, as discussed in the text. Since a smooth Pt electrode was used, the geometrical and real surface areas are about the same.

*3.3.2.4. Oer Tafel slopes obtained in the presence of $(COOH)_2$.* The use of porous, high surface area electrodes can result in the enhancement of the observed rates of activation controlled reactions. However, particularly for thick and high surface area electrodes, mass transport limitations within the high surface area, porous film structure may become a problem. This could result in an experimentally observed reaction rate constant which is less and less dependent on the applied potential as the film thickness increases. In effect, an increasingly smaller fraction of catalytic sites within the oxide are utilized for the $(COOH)_2$ oxidation reaction with increasing potential, when the reaction is limited by mass transport within the oxide film. This, in turn, suggests that with increasing potential an increasing number of sites may be available for the oer for such a mass transport limiting case (assuming that the organic oxidation reaction is preferred over the oer, see below). Therefore, the current due to the oer would increase more rapidly than predicted by the 60 mV $dec^{-1}$ Tafel slope observed for the oer in the organic free $H_2SO_4$ solution. This behavior should result in a smaller than 60 mV $dec^{-1}$ Tafel slope for the oer in the presence of $(COOH)_2$, at least when mass transport limitations play a role. To address this issue, the current densities due to the oer ($J_{O_2}$'s) were calculated from experimental anodic electrolysis data obtained for 20 ml's of the initially $10^{-3}$ M $(COOH)_2$ in 0.5 M $H_2SO_4$ solutions carried out at different potentials (see above). The $J_{O_2}$ values were calculated by subtracting the average current density due to $(COOH)_2$ oxidation to $CO_2$ from the average monitored current density. All current density values were averaged for the initial 1.5 h period of the anodic electrolysis experiments. The current density due to $(COOH)_2$ to $CO_2$ oxidation was estimated from the experimentally observed $c(COOH)_2$ changes during the same 1.5 h electrolysis time period using Faraday's law. Fig. 9 shows the dependence of the applied potentials versus the $\log(J_{O_2})$ data obtained in this manner for two $Pt/WO_x$ anodes of 58 and 76 $cm^2$ real Pt area. The data suggests, even though only four potentials are investigated, that for each electrode a linear relationship between the applied potential and the $\log(J_{O_2})$ value exists. The 'Tafel' slopes for the oer in the presence of $(COOH)_2$ estimated in this manner for the two $Pt/WO_x$ anodes are found to be 63 and 71 mV $dec^{-1}$, as indicated in Fig. 9. These values are considered to be close to the 60 mV $dec^{-1}$ slope found for the oer in the organic free 0.5 M $H_2SO_4$ solution for $Pt/WO_x$ anodes (Fig. 3), and certainly do not indicate a decrease in the

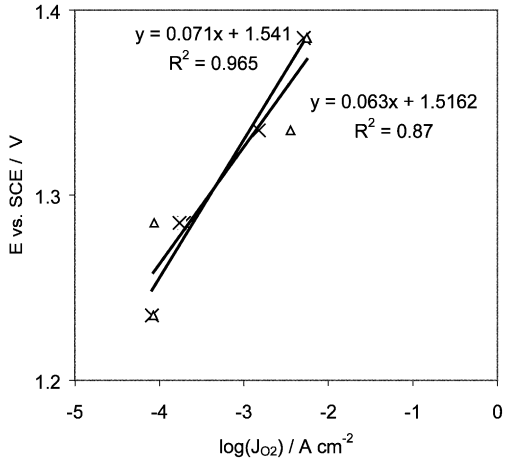


Fig. 9. 'Tafel' plots for the $O_2$ evolution reaction (oer) for a (△) 130 $cm^2$ real Pt area and (×) 58 $cm^2$ real Pt area Pt/$WO_x$ anode in the presence of $(COOH)_2$. The current density value for the oer ($J_{O_2}$) is the average value estimated during the first hour of electrolysis of 20 ml's of initially $10^{-3}$ M $(COOH)_2$ in 0.5 M $H_2SO_4$ solutions. The $J_{O_2}$ values were obtained by subtracting the theoretical average current density for the $(COOH)_2$ to $CO_2$ oxidation (calculated from experimentally observed $c(COOH)_2$ changes, as described in the text) from the average current density monitored during the first 1.5 h of electrolysis. The solutions were rigorously stirred, as described in the text.

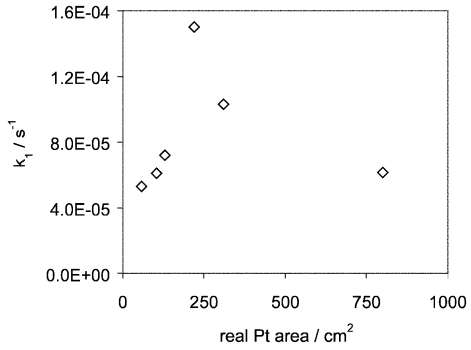


Fig. 10. First order reaction rate constants ($k_1$ values) found for different real Pt areas Pt/$WO_x$ anodes. The $k_1$ values were estimated from the slope of $\ln(c_o/c_{(t)})$ vs. the electrolysis time plots obtained for 20 ml's of initially $10^{-3}$ M $(COOH)_2$ in 0.5 M $H_2SO_4$ solutions at 1.285 V vs. SCE. (An MSE was used in the actual experiments.) $c_o$ is the initial $(COOH)_2$ concentration and $c_{(t)}$ is the $(COOH)_2$ concentration at a particular electrolysis time, $t$. The solutions were rigorously stirred, as described in the text.

Tafel slope. The results are therefore consistent with an activation controlled mechanism of the $(COOH)_2$ oxidation reaction studied here.

It should be noted that at a particular potential, the $J_{O_2}$ values estimated in the presence of the $10^{-3}$ M $(COOH)_2$ are ca. 10 times smaller than the $J_{O_2}$ values observed in the organic free 0.5 M $H_2SO_4$ background solution. It is possible that $H_2O$ and $(COOH)_2$ compete for the same catalytic film sites resulting in the observed suppression of the $O_2$ evolving reaction by $(COOH)_2$.

*3.3.2.5. The $k_1$ values for Pt/$WO_x$ anodes of different real Pt surface areas and film thicknesses.* $k_1$ values were also estimated for Pt/$WO_x$ anodes made of different real Pt surface areas. The Pt/$WO_x$ anodes were prepared by depositing the oxide films for different times, thus resulting in oxide films of different thicknesses and real Pt areas. Deposition times varied between 10 min and 6 h. The geometrical area of the Pt/$WO_x$ anodes employed was 0.98 $cm^2$ and 20 ml's of initially $10^{-3}$ M $(COOH)_2$ in 0.5 M $H_2SO_4$ solutions were used for the electrolysis studies. All electrolysis experiments were carried out at 1.285 V. Fig. 10 shows a plot of the $k_1$ values as a function of the real Pt area for several Pt/$WO_x$ anodes of different film thicknesses. As expected for an activation controlled reaction, the $k_1$ value is seen to consistently increase with increasing Pt area, i.e. with increasing oxide film thickness, for the tested Pt/$WO_x$ anodes up to 230 $cm^2$ real Pt area. The largest $k_1$ value of $1.5 \times 10^{-4}$ $s^{-1}$ was found for the (230 $cm^2$ real Pt area) Pt/$WO_x$ anode. In this particular case, the $J_{exp}$ value (based on the geometrical area) was found to be close to the same as the limiting current density value calculated for a mass transport controlled reaction using Eq. (3) and diffusion coefficient and diffusion layer thickness values of $5 \times 10^{-6}$ $cm^2$ $s^{-1}$ and 15 μm, respectively. Therefore, this $k_1$ value of $1.5 \times 10^{-4}$ $s^{-1}$ is believed to represent the limiting, largest possible reaction rate constant value for the oxalic acid oxidation carried out under the conditions employed here. This means that the limiting current does not increase as the film thickness increases, i.e. that the diffusion layer thickness is large in comparison with roughness. This means that an increase in the Pt/$WO_x$ anode film thickness will most probably not result in larger $k_1$ values, i.e. will not further increase the rate for the $(COOH)_2$ oxidation reaction. However, it will likely result in a decrease of the current efficiency for this oxidation reaction, as more film sites are available for the oer, which is still an activation controlled reaction. This, in turn, suggests that the fraction of the current due to the oer increases as the Pt/$WO_x$ film thickness exceeds the 'limiting value' for the organic oxidation. The fact that the $k_1$ values for the two very large surface area anodes are smaller than the limiting $k_1$ value is possible due to morphological differences within these oxide anodes and/or IR effects within the oxide structure. This behavior is not further investigated in the present work.

*3.3.2.6. Suggested mechanism for the anodic $(COOH)_2$ oxidation reaction using Pt/$WO_x$ anodes.* The observed lack of dependence of the first order rate constant for the activation controlled $(COOH)_2$ oxidation reaction on potential (Table 2) can be explained in terms of a

chemical reaction of $(COOH)_2$ with the $Pt/WO_x$ anode surface. This chemical reaction needs to be the rate determining step in the $(COOH)_2$ to $CO_2$ oxidation reaction. An initial, rate determining chemical reaction of $(COOH)_2$ with the $Pt/WO_x$ anode surface, i.e. a chemical reaction that precedes any faradaic charge transfer reactions involving this organic acid, theoretically results in a potential independent oxidation rate constant value. However, such a reaction is difficult to visualize based on 'chemical' reasoning and, hence, this possibility is not further considered. A more likely oxidation mechanism could involve the partial electrochemical oxidation of $(COOH)_2$ that is accompanied by de-protonation, as suggested in Eq. (4) below. This electrochemical oxidation reaction is suggested to result in the adsorption of the partially oxidized form of the organic onto the $Pt/WO_x$ anode surface (S). Formation of $CO_2$ can then occur via a chemical reaction that is responsible for the breaking of the carbon–carbon bond of the adsorbed form of the oxalic acid, as suggested in Eq. (5), as follows:

$$2S + (HOOC)_2 \leftrightarrow S_2(OOC)_{2(ads)} + 2H^+ + 2e^- \quad (4)$$

$$S_2(OOC)_{2(ads)} \rightarrow 2S + 2CO_2 \quad (5)$$

This oxidation mechanism is analogous with the homogenous solution oxidation reaction of $(COOH)_2$ to $CO_2$ that involves Pb(+IV) or Mn(+VII) ion as oxidizing agent [16,17]. Both of these oxidizing agents catalyze the breaking of the carbon–carbon bond by forming a chelate type intermediate complex with the organic [16,17]. Therefore, it appears reasonable to suggest that this reaction, i.e. the breaking of the carbon–carbon bond that has a high activation energy, is rate determining in the anodic $(COOH)_2$ oxidation reaction studied in this work. It should also be noted that the $(COOH)_2$ oxidation reaction to $CO_2$ does not theoretically need oxygen species supplied by foreign sources. Thus, there may be little or no involvement of 'hydroxy radicals' in the $(COOH)_2$ oxidation reaction, in contrast to the mechanism suggested for other organic oxidation reactions using e.g. electrode materials like antimony doped $SnO_2$ [4].

A well known reaction for which the reaction rate constant is independent of potential can be observed for the $H_2$ evolution reaction (her) [13,18,19]. One possible reaction mechanism suggested for the her is the 'catalytic pathway', as shown below for a particular electrode surface (S) [18,19]:

$$S + H^+ + e^- \rightarrow MH_{ads} \quad (6)$$

$$2SH_{ads} \rightarrow S + H_2 \quad (7)$$

It has been discussed in prior work that the reaction rate constant for the her is independent of the potential when the chemical recombination reaction of the surface adsorbed H (Eq. (6)) is rate determining and when the surface coverage of the adsorbed H approaches 1. Therefore, this particular case of the her is similar to the proposed mechanism for the anodic oxidation of $(COOH)_2$ using $Pt/WO_x$ anodes (Eqs. (4) and (5)). Furthermore, the $(COOH)_2$ oxidation data obtained in this work may suggest that the coverage of the adsorbed form of the oxalic acid ($\theta$) onto the catalytic sites of the $Pt/WO_x$ anode is very high, possibly approaching a value of 1. The high $\theta$ value may explain the fact that very high current efficiency values are achieved for the $(COOH)_2$ to $CO_2$ oxidation.

## 4. Conclusions and summary

In this work, the anodic oxidation of $(COOH)_2$ was studied in detail using $Pt/WO_x$ anodes. $Pt/WO_x$ anodes of different real Pt areas and oxide film thicknesses were made from tungsten and platinum containing solutions employing an electrochemical deposition method. The resulting films are shown to be very porous and possess a sandstone like structure likely allowing access of the electrolyte solution deep into the oxide film. Typical features for polycrystalline Pt are seen in the cyclic voltammogams for these $Pt/WO_x$ electrodes recorded in 0.5 M $H_2SO_4$ at potentials below the $O_2$ evolution reaction. Current–voltage measurements for the oer carried out in 0.5 M $H_2SO_4$ indicated two Tafel slope regions for the $Pt/WO_x$ anodes, namely a slope of 60 mV $dec^{-1}$ at lower potentials and a slope of ca. 320 mV $dec^{-1}$ at very positive potentials. The latter very large Tafel slope may indicate the formation of a resistive film on the titanium that is used as substrate for the $WO_x$ based films and, hence, the use of these $WO_x$ based anodes at very positive potentials was avoided. The Tafel slope of 60 mV $dec^{-1}$ observed at lower potentials is different from the 120 mV $dec^{-1}$ Tafel slope observed for the oer using polycrystalline Pt electrodes. These results indicate that at more positive potentials, i.e. in the oer region, the catalytic behavior for the oer, and maybe also for the oxidation of organics, is different for $Pt/WO_x$ and polycrystalline Pt electrodes.

It was shown that $(COOH)_2$ is readily oxidized using the $Pt/WO_x$ anodes. In fact, current-density/time profiles suggest that the anodic $(COOH)_2$ oxidation reaction is more rapid than observed for antimony doped $SnO_2$ anodes. This suggests that the $WO_x$ based anodes used in this work are very promising catalysts for the anodic $(COOH)_2$ oxidation reaction. It was shown that the $(COOH)_2$ oxidation reaction takes place under activation controlled conditions, even for high ($>100$ $cm^2$) real Pt surface area $Pt/WO_x$ anodes. Beyond about 200 $cm^2$ real Pt surface area, problems associated with mass-transport limitations and possibly also pore blocking arise. It was also found that the $(COOH)_2$ depresses the oer. The nature of the catalytic sites for the

$(COOH)_2$ oxidation reaction within these $Pt/WO_x$ films has not yet been identified. Rate constants and half lives for the activation controlled $(COOH)_2$ oxidation reaction were obtained as a function of the applied potential for the $Pt/WO_x$ anodes. The reaction rate constant and half life values for the anodic $(COOH)_2$ oxidation reaction were found to be independent of potential. Based on this behavior, an oxidation mechanism similar to the 'catalytic pathway' for the $H_2$ evolution reaction is suggested, i.e. it is believed that a chemical reaction is the rate-determining step. Furthermore, the anodic $(COOH)_2$ oxidation mechanism suggested in this work is believed to involve adsorptive interactions of $(COOH)_2$ with the $Pt/WO_x$ anode surface and that the surface coverage of the organic is high, approaching values of 1.

## Acknowledgements

The authors wish to thank Dr E. Gileadi (Tel-Aviv University, Isreal) and Dr Y. Kargin (Kazan State University, Russia) for helpful discussions. Assistance from P. L'Abbe (National Research Council Canada) for making the glass cells used in this work and G. Pleizier (National Research Council Canada) for the SEM work is also greatly acknowledged.

## References

[1] R. Kotz, S. Stucki, B. Carcer, J. Appl. Electrochem. 21 (1991) 14.
[2] C. Comninellis, Electrochim. Acta 39 (1857) 1994.
[3] J. Feng, D.C. Johnson, J. Electrochem. Soc. 138 (1991) 3328.
[4] O. Simond, V. Schaller, C. Comninellis, Electrochim. Acta 42 (1997) 2009.
[5] M. Gatrell, D. Kirk, J. Electrochem. Soc. 139 (1992) 2736.
[6] C. Bock and B. MacDougall, Electrochim. Acta 47 (2002) 3361.
[7] P.K. Shen, A.C.C. Tseung, J. Electrochem. Soc. 11 (1994) 3082.
[8] B. Correa-Lozano, C. Comninellis, A. DeBattisti, J. Appl. Electrochem. 27 (1997) 970.
[9] B.E. Conway, H. Angerstein-Kozlowska, Acc. Chem. Res. 14 (1981) 49.
[10] A. Damjanovic, A. Dey, J.O'M. Bockris, Electrochim. Acta 11 (1966) 791.
[11] B.E. Conway, T.C. Liu, G. Jerkiewicz, in: R.R. Adzic, F.C. Anson, K. Kinoshita (eds.), Oxygen Electrochemistry 1995, PV-95-26, The Electrochemical Society Proceeding Series, Pennington, NJ, 1996, p. 132.
[12] V.A. Alves, L.A DaSilva, J.F.C. Boodts, S. Trasatti, Electrochim. Acta 39 (1994) 1585.
[13] E. Gileadi, Electrode Kinetics for Chemists, Chemical Engineers, and Material Scientists, VCH Publishers Inc, New York, 1993, p. 60.
[14] H. Kuchling, Physik, Formeln und Gesetze, Buch- and Zeit-Verlagsgesellscahft mbH Koeln, 1982.
[15] A.J. Bard, L.R. Faulkner, Electrochemical Methods, Fundamentals and Applications, John Wiley & Sons, Inc, New York, 1980, p. 218.
[16] L.F. Fieser, M. Fieser, Advanced Organic Chemistry, 5th ed., Reinhold Publishing Corporation, New York, 1965, p. 130.
[17] C. Bock, B. MacDougall, J. Electrochem. Soc. 146 (1999) 2925.
[18] B.E. Conway, L. Bai, J. Electroanal. Chem. 198 (1986) 149.
[19] M. Elam, B.E. Conway, J. Appl. Electrochem. 17 (1987) 1002.